Journal of Magnetic Resonance 214 (2012) 221–226

Contents lists available at SciVerse ScienceDirect

Journal of Magnetic Resonance

journal homepage: www.elsevier.com/locate/jmr

X-band rapid-scan EPR of nitroxyl radicals

Deborah G. Mitchell [b], Richard W. Quine [a], Mark Tseitlin [b], Sandra S. Eaton [b], Gareth R. Eaton [b,*]

[a] School of Engineering and Computer Science, University of Denver, United States
[b] Department of Chemistry and Biochemistry, University of Denver, Denver, CO 80208, United States

ARTICLE INFO

Article history:
Received 8 October 2011
Revised 9 November 2011
Available online 20 November 2011

Keywords:
Deconvolution
Nitroxyl radicals
Rapid scan EPR
Resonator *Q*

ABSTRACT

X-band rapid-scan EPR spectra were obtained for dilute aqueous solutions of nitroxyl radicals ^{15}N-mHCTPO (4-hydro-3-carbamoyl-2,2,5,5-tetra-perdeuteromethyl-pyrrolin-1-^{15}N-oxyl-d_{12}) and ^{15}N-PDT (4-oxo-2,2,6,6-tetra-perdeuteromethyl-piperidinyl-^{15}N-oxyl-d_{16}). Simulations of spectra for ^{15}N-mHCTPO and ^{15}N-PDT agreed well with the experimental spectra. As the scan rate is increased in the rapid scan regime, the region in which signal amplitude increases linearly with B_1 extends to higher power and the maximum signal amplitude increases. In the rapid scan regime, the signal-to-noise for rapid-scan spectra was about a factor of 2 higher than for unbroadened CW EPR, even when the rapid scan spectra were obtained in a mode that had only 4% duty cycle for data acquisition. Further improvement in signal-to-noise per unit time is expected for higher duty cycles. Rapid scan spectra have higher bandwidth than CW spectra and therefore require higher detection bandwidths at faster scan rates. However, when the scan rate is increased by increasing the scan frequency, the increase in noise from the detection bandwidth is compensated by the decrease in noise due to increased number of averages per unit time. Because of the higher signal bandwidth, lower resonator *Q* is needed for rapid scan than for CW, so the rapid scan method is advantageous for lossy samples that inherently lower resonator *Q*.

1. Introduction

Rapid scan is an electron paramagnetic resonance (EPR) method in which the magnetic field is scanned through resonance in a time that is short relative to T_2 [1,2], and the absorption and dispersion signals are recorded by direct detection. Phase-sensitive detection at the magnetic field modulation frequency is not used. Oscillations are observed on the trailing edge of the signal. Rapid scan signals obtained with either triangular or sinusoidal scans can be deconvolved to give the conventional spectra [3,4].

Previously, rapid field scan EPR experiments were performed at 250 MHz (VHF) on a triarylmethyl (trityl) radical ($T_2 \sim 11.5$ μs) and on deoxygenated lithium phthalocyanine (LiPc) ($T_2 \sim 2.5$ μs) [4–7]. Because of the relatively long T_2 values for these samples, rapid scan conditions could be achieved with scan rates as low as 6 kG/s. The advantages of rapid scan EPR at X-band for the E′ center in irradiated fused quartz ($T_2 \sim 100$ μs) [8] and for α,γ-bisdiphenylene-β-phenylallyl (BDPA, $T_2 \sim 100$ ns) [9] have been demonstrated.

This paper reports the application of X-band rapid scan EPR to nitroxyl radicals. Nitroxyl radicals were selected for study because of their widespread use as spin probes in biomedical applications [10,11]. The two prior rapid field scan reports for nitroxyl radicals were at 250 MHz [12,13]. Rapid frequency scans for nitroxyls have been reported at W-band [14]. In dilute deoxygenated aqueous solutions at ambient temperature, nitroxyl radicals have T_2 values in the range of 500–700 ns [15]. These values of T_2 are much shorter than for trityl, LiPc, or irradiated fused quartz samples, so the scan rates required to achieve the rapid scan regime for nitroxyls are much faster. Sinusoidal scans with resonated coils allow the magnetic field to be swept at much higher rates than with triangular scans [9], which allows samples with shorter T_2 to be measured in the rapid scan regime. The nitroxides selected for study were ^{15}N-PDT (4-oxo-2,2,6,6-tetra-perdeuteromethyl-piperidinyl-^{15}N-oxyl-d_{16}), because of its narrow lines [15], and ^{15}N-mHCTPO (4-hydro-3-carbamoyl-2,2,5,5-tetra-perdeuteromethyl-pyrrolin-1-^{15}N-oxyl-d_{12}), because of its utility for oximetry imaging [16].

2. Methods

2.1. Sample preparation

^{15}N-PDT with 98% isotope purity was purchased from CDN Isotopes (Quebec, Canada). ^{15}N-mHTCPO was prepared as previously described [17] and provided by Prof. Halpern (University of Chicago). Solutions in 80/20 EtOH/H_2O were 0.2 mM for ^{15}N-PDT and 0.1 mM for ^{15}N-mHTCPO. These concentrations are in a range where the contribution to relaxation from collisions is very small [15]. The samples, in 4 mm o.d. × 3 mm i.d. quartz tubes, had heights of 3 mm, resulting in 3 × 3 mm cylindrical shapes. The

* Corresponding author. Fax: +1 303 871 2243.
E-mail address: geaton@du.edu (G.R. Eaton).

1090-7807/$ - see front matter © 2011 Elsevier Inc. All rights reserved.
doi:10.1016/j.jmr.2011.11.007

height was selected to decrease the impact of distortions in the signal due to nonuniformities in the rapidly-scanned fields. Both samples were degassed by performing six freeze–pump–thaw cycles and then the tubes were flame sealed.

2.2. EPR spectroscopy

CW spectra and rapid scan signals were obtained on a Bruker custom E500T X-band spectrometer. The microwave bridge had bandwidth options of 20 or 200 MHz. Signal acquisition was via a Bruker signal processing unit (SPU) for CW spectra and a SpecJetII fast digitizer for rapid scan signals. For CW spectra the modulation frequency and amplitude were chosen to minimize lineshape distortions. A critically-coupled FlexLine ER4118X-MD5 dielectric resonator was used to minimize eddy currents induced by the rapidly-changing magnetic fields. Resonator Q was measured using the pulse ring down method with a locally-designed addition to the bridge [18]. The 80/20 EtOH/H_2O solutions lowered the resonator Q to about 150, which corresponds to a resonator 3 dB bandwidth of 64 MHz at about 9.7 GHz (Eq. (1)).

$$\mathrm{BW_{res}} = \frac{\upsilon}{Q} \tag{1}$$

where υ is the resonator frequency. In a rapid scan experiment, the field is sequentially scanned up or down, so only half of the resonator bandwidth is available for the signal in either half cycle. The resonator Q that is required to minimize distortion of a signal with a bandwidth $\mathrm{BW_{signal}}$ is:

$$Q = \frac{\upsilon}{2\mathrm{BW_{signal}}} \tag{2}$$

where $\mathrm{BW_{signal}}$ is approximately:

$$\mathrm{BW_{signal}} \approx \frac{Na\gamma T_2^*}{2\pi} \tag{3}$$

where N was set to 5 (which accounts for five time constants for the approximately exponential T_2^* decay), a is the scan rate in G/s (Eq. (4)), and γ is the gyromagnetic ratio for an electron. Although the rapid scan regime is defined in terms of T_2, calculation of signal bandwidth requires inclusion of inhomogeneous broadening and is expressed in terms of T_2^*. For hyperfine split spectra and other complex lineshapes an approximate T_2^* based on the overall rate of damping of the FID should be used in Eq. (3). The goal is to avoid filtering out the high-frequency components of the spectrum. A more precise estimate of signal bandwidth can be obtained by Fourier transformation of the rapid scan signal taken under conditions of high system bandwidth.

A locally-designed magnetic field scan driver created sinusoidal scans with 9.5 cm diameter circular coils outside the resonator, aligned coaxially with the main magnetic field. To avoid excessive heating of the amplifier in the scan driver, the sine wave for the magnetic field scans was generated in bursts with a duty cycle of 33% or 50%. To permit equilibration of the hardware and spin response, the rapid scan signals were digitized only after the 5th cycle of each burst, which corresponds to a duty cycle for data acquisition of about 4%. The center field of the scan was selected to be close to resonance. In a sinusoidal scan, the scan rate is a function of the offset from the center of the scan. Scan rates were designated by the rate at the center, which is given by Eq. (4),

$$\mathrm{rate} = \pi w f \tag{4}$$

where w is the width of the scan in gauss and f is the scan frequency.

The scan frequency ranged from 10 to 60 kHz, and scan widths ranged from 5 to 60 G. The rapid scan signal, after multiplication by the sinusoidal driving function, is the convolution of the slow scan spectrum with the driving function [3]. The slow scan spectra were recovered by deconvolution, using the Fourier transforms of the data and the driving function [3]. The up- and down-field half cycles of the sinusoidal scans were analyzed separately. To facilitate comparison with conventional CW spectra, a pseudomodulation procedure [19] was used to calculate the first derivative spectrum. This procedure included a fourth-order low pass Butterworth filter [20]. Filtering was done with the MatLab "butter" routine and the value of the adjustable parameter, W_n, was selected to give less than 2% broadening ($W_n = 0.12$).

The T_1 and T_2 for ^{15}N-PDT and ^{15}N-mHCTPO in 80/20 EtOH/H_2O were measured using three-pulse inversion recovery and two-pulse electron spin echo decay, respectively, on a locally-built pulsed spectrometer [21]. The T_2 values for the low field lines of ^{15}N-mHCTPO and ^{15}N-PDT are 0.70 and 0.61 μs, respectively. The T_1 values for the low field line of ^{15}N-mHCTPO and ^{15}N-PDT are 1.2 and 0.79 μs, respectively. The estimated uncertainties for T_1 and T_2 are about 3%. The T_2^* for ^{15}N-PDT, measured from a single pulse FID, was 0.43 ± 0.03 μs. This value of T_2^* is about 13% larger than would have been calculated using the expression.

$\Delta B_{\mathrm{pp}}\,(\mathrm{G}) = 6.56 \times 10^{-8}\,(\mathrm{G\,s})/T_2\,(\mathrm{s})$, which approximates the inhomogeneously broadened ΔB_{pp} (0.175 G) as a Lorentzian. For ^{15}N-mHCTPO the partially resolved ring proton hyperfine coupling causes a more complicated decay of the FID, so $T_2^* = 0.26$ μs was estimated from the inhomogeneously broadened linewidth of ΔB_{pp} (0.256 G).

2.3. Power saturation

The amplitudes of the deconvolved lines were measured as a function of source power for a series of scan rates. For ^{15}N-mHCTPO, the scan width was held constant while the scan frequency was varied. To demonstrate an alternate approach to varying scan rates the scan frequency for ^{15}N-PDT was held constant, and scan widths were varied. The power saturation curves were measured multiple times and signal amplitudes obtained for the same incident power were averaged.

2.4. Characterization of noise

The standard deviation of the noise in the center of deconvolved spectra was measured as a function of source power. For three replicate data sets the noise was independent of power below ~50 mW. From 50 to 200 mW there was an increase in noise of about 33%. These results indicate that for powers greater than about 50 mW, the noise is dominated by the source. As resonator Q increases, source noise becomes significant at lower powers [22]. Because a low Q (~150) was used for the rapid scan experiments, the source noise only becomes significant at very high powers.

2.5. Determination of resonator efficiency

The resonator efficiency, Λ, is the conversion efficiency of incident power to B_1, the microwave magnetic field amplitude at the sample. For the ^{15}N-mHCTPO sample, $\Lambda = 0.5$ G/$\sqrt{}$watt was determined by simulating a CW power saturation curve with SATMON, a locally-written Fortran program [23]. Since Λ is proportional to $\sqrt{Q}$, the value is dependent on sample size, positioning, and resonator tuning. To fit the rapid scan power saturation curves for the ^{15}N-mHCTPO sample, Λ ranged from 0.38 to 0.45 G/$\sqrt{}$watt.

2.6. Simulations

Simulations of the rapid scan signals were performed by numerical integration of the Bloch equations and summation of

the contributions from multiple spin packets. The input parameters were magnetic field scan width, scan frequency, resonator Q, offset of the center of the scan from the resonant magnetic field, T_1, T_2, and B_1. Two approaches were used to determine the weightings of the spin packets that model the inhomogeneous broadening. (i) For spectra obtained with small enough B_1 that saturation effects were negligible, the inhomogeneous broadening was approximated by a set of spin packets with relative amplitudes calculated using a Voigt function [4]. The parameters for the Voigt function were determined by fitting the rising edge of the signal. An uncertainty of about ±7% was estimated for the inhomogeneous broadening. (ii) For the power saturation curves the known deuterium hyperfine splittings [15] were used to calculate the positions of individual spin packets relative to the center of the spectrum. The field offsets for the centers of the spectra were measured from the experimental rapid scan spectra obtained by deconvolution. Changes in offsets within a data set were attributed to frequency drift arising from changes in the temperature of the resonator. The simulated rapid scan spectra were deconvolved, and the amplitudes were measured. The calculations were performed for each experimental combination of scan width and scan frequency. To determine the dependence of the maximum amplitude in the power saturation curve on scan rate, power saturation curves also were simulated for scan rates between 300 kG/s and 10 MG/s.

3. Results

The rapid scan spectra of ^{15}N-PDT (Fig. 1) exhibit characteristic oscillations on the trailing edge of the signal. The values of T_2 obtained by simulation of the spectra were in good agreement with values obtained directly by spin echo.

The slow scan absorption spectrum for ^{15}N-PDT was obtained from the data in Fig. 1 by deconvolution. For comparison with the conventional spectrum, pseudomodulation was used to calculate the first-derivative, which is in good agreement with the CW spectrum (Fig. 2).

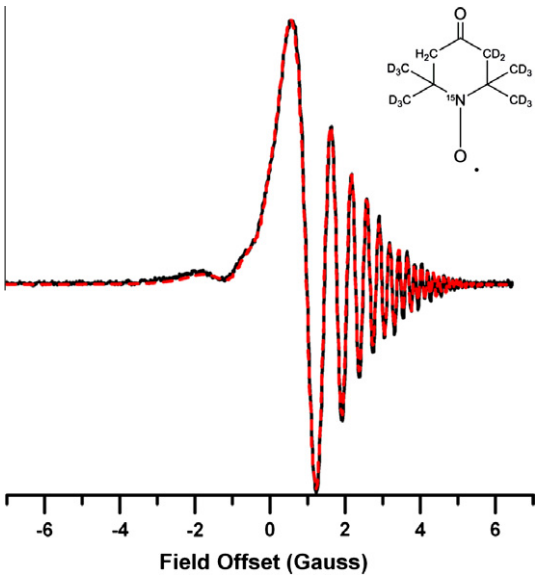

Fig. 1. (black line) Segment of an X-band sinusoidal rapid scan spectrum of the low-field nitrogen hyperfine line for a degassed 0.2 mM ^{15}N-PDT solution, obtained with 55 G scan width, 3419 G center field, and 29.7 kHz scan frequency (scan rate ~5.1 MG/s). 1024 averages were collected with resonator $Q \sim 150$ and 2 mW power (B_1 = 0.02 G), which is well below the peak in the power saturation curve. (red dashed line) Simulation obtained with T_2 = 0.61 μs and 75 mG inhomogeneous broadening. (For interpretation of the references to color in this figure legend, the reader is referred to the web version of this article.)

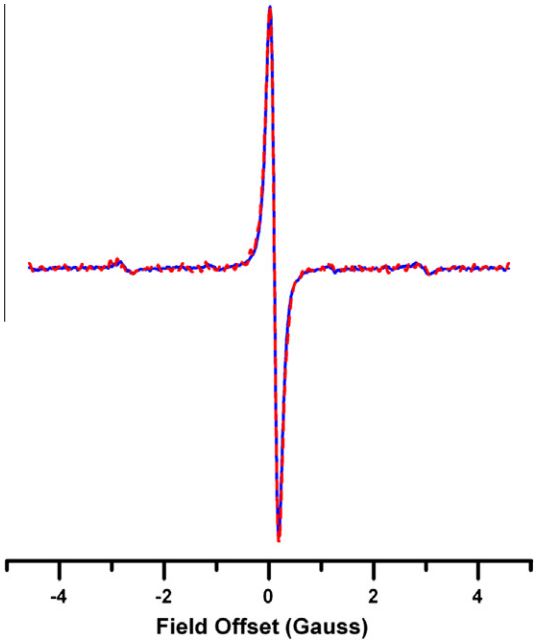

Fig. 2. Segments of spectra of the low-field nitrogen hyperfine line for degassed 0.2 mM ^{15}N-PDT solution. (blue line) CW spectrum obtained with 45 G sweep width, 0.02 G modulation amplitude, 82 s scan time, and 0.3 mW power. (red dashed line) Pseudomodulated, deconvolved rapid scan spectrum obtained with 9.15 G scan width, and 29.7 kHz scan frequency (scan rate of ~0.85 MG/s). 1024 averages were collected in ~1 s. with resonator $Q \sim 150$ and 2 mW power (B_1 = 0.02 G). (For interpretation of the references to color in this figure legend, the reader is referred to the web version of this article.)

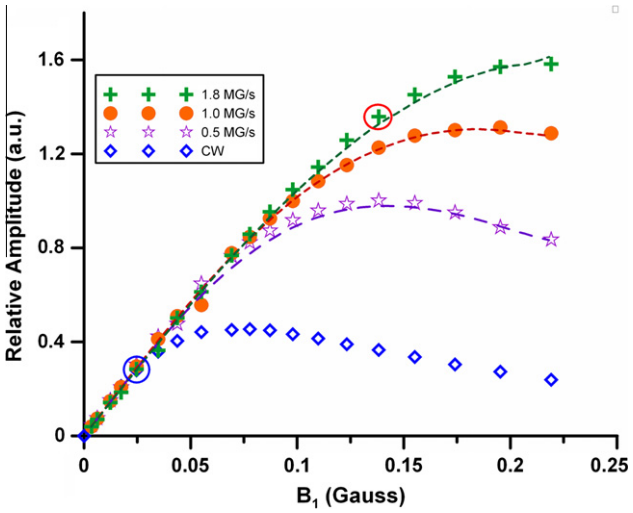

Fig. 3. Amplitude of CW and rapid scan spectra of the low-field nitrogen hyperfine line of 0.1 mM ^{15}N-mHCTPO solution as a function of microwave B_1. The scan widths were ~10 G and rapid scan frequencies were 15.9, 31.5, or 57.4 kHz. Rapid-scan signals were 1024 averages, collected in less than 1 s. CW spectra were collected with single scan acquired in ~82 s. The y-axis scale is the same for all of the rapid scans. The amplitude of the CW spectra is scaled to match that obtained for the rapid scans at low B_1. The dashed lines represent the calculated power saturation curves, which were simulated by solving the Bloch equations. The point that corresponds to the acquisition conditions for the spectra shown in Fig. 6A–C is circled in red, and the point that corresponds to the low-power CW spectrum in Fig. 6D is circled in blue. (For interpretation of the references to color in this figure legend, the reader is referred to the web version of this article.)

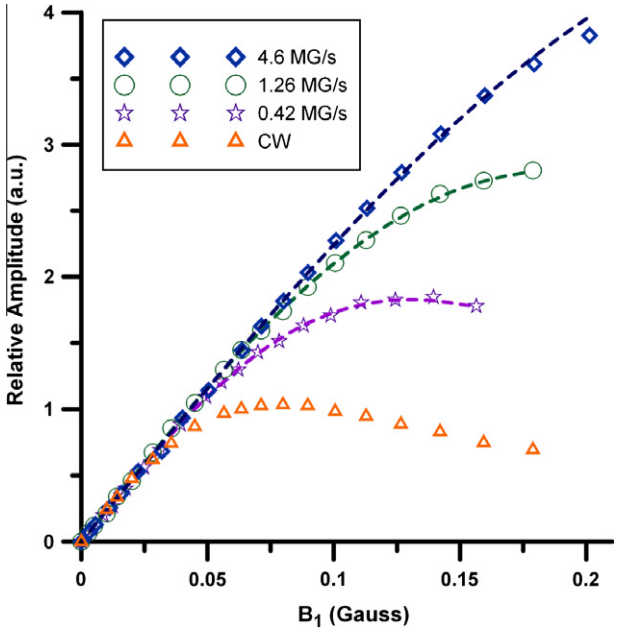

Fig. 4. Amplitude of CW and rapid scan spectra of the low-field nitrogen hyperfine line for 0.2 mM ^{15}N-PDT solution as a function of microwave B_1. The rapid scan frequency was ~30 kHz and the scan width was varied. Rapid-scan signals were 1024 averages, collected in less than 1 s. CW spectra were single scans, collected in ~82 s. The *y*-axis scale is the same for all of the rapid scans. The dashed lines represent the calculated power saturation curves, which were simulated by solving the Bloch equations. The amplitude of the CW spectra is scaled to match that obtained for the rapid scans at low B_1.

3.1. Power saturation

The experimental and calculated dependence of the amplitude of the rapid scan signals on microwave power for ^{15}N-mHCTPO for three rapid scan rates is significantly different than for a CW spectrum (Fig. 3). In rapid scan EPR the magnetic field is on resonance for a shorter time than in conventional CW spectroscopy, so the energy absorbed by the spins is less, for the same B_1, and the spectrum does not saturate as readily. As the scan rate is increased, the region in which the signal amplitude increases linearly with power extends to higher power and the maximum signal amplitude increases (Fig. 3). A similar dependence of power saturation on scan rate was observed for ^{15}N-PDT (Fig. 4).

The maximum signal amplitudes in simulated power saturation curves as a function of scan rate for ^{15}N-mHCTPO are shown in Fig. 5A. The definition of the rapid scan regime is that the time for passage through resonance is short relative to T_2. The regime in which the rapid scan signal amplitude is enhanced is defined by Eq. (5), which points out that higher powers can be used for faster scans.

$$\frac{B_1}{\left(\frac{dB_0}{dt}\right)(T_1T_2)^{0.5}} < 1 \tag{5}$$

where dB_0/dt is the scan rate [1,7,24]. The maximum amplitude in the calculated power saturation curves becomes dependent on scan rate (Fig. 5A) when the left hand side of Eq. (5) decreases below 1, which confirms that the benefit of scanning faster occurs within the rapid scan regime. At log(rate) ~ 7, the maximum amplitude of the power saturation curve begins to decrease (Fig. 5A). The decrease in amplitude is observed at this rate because of relaxation time limitations. If the scan rate is too fast, the magnetization has not fully come to equilibrium before the next excitation. To achieve the increased signal amplitudes at higher scan rates requires higher B_1 (Fig. 5B).

The signal-to-noise per unit time for CW and rapid scan was compared for the ^{15}N-mHCTPO sample (Fig. 6). The power, modulation amplitude, and a fourth-order low pass Butterworth filter setting for the CW spectrum were selected to cause no more than ~2% broadening (W_n = 0.11). The conversion time selected for the CW experiment was 0.9 ms for 1024 points to give a sweep time of 0.92 s. The rapid scan data with the fastest rate shown in Fig. 3 (1.8 MG/s) was chosen for the comparison. The power and Butterworth filter setting for the rapid scan spectrum were selected to also limit signal broadening to ~2%. The ~57 kHz scan frequency allowed 1024 scans to be averaged in 0.9 s. The rapid scan and CW experiments had about the same data acquisition time, and filter bandwidths appropriate for each scan were selected, so the *S*/*N* was compared directly. By using rapid scan EPR, the *S*/*N* was improved by about a factor of 2 (Fig. 6).

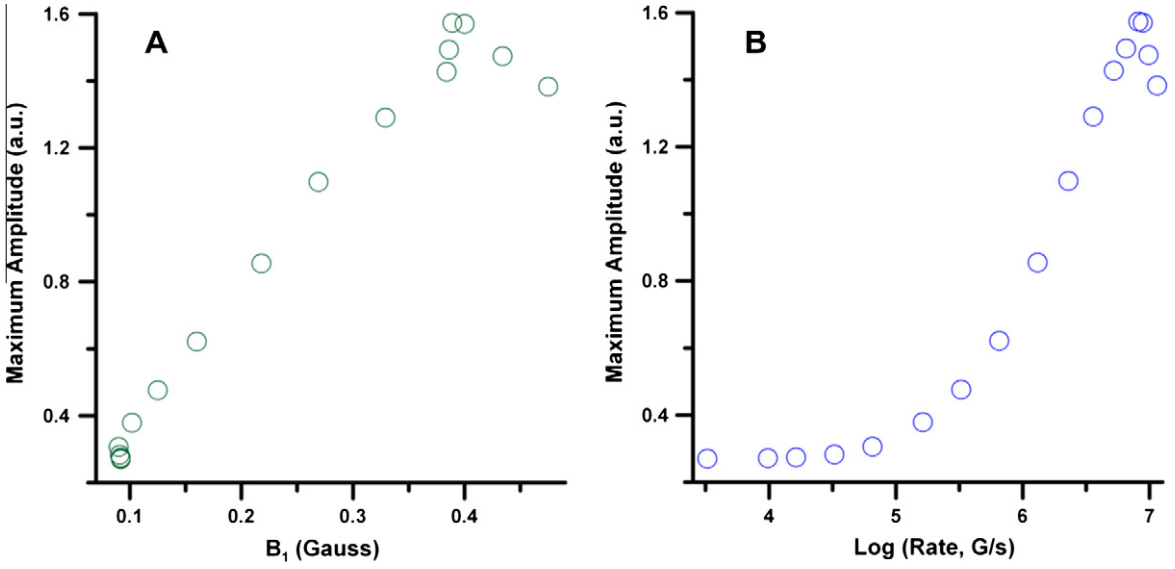

Fig. 5. Simulation for ^{15}N-mHCTPO of the maximum intensities in the power saturation curves as a function of rate (A). The B_1 required to achieve these amplitudes is shown in (B). Scan width was ~10 G and scan frequency was varied from 0.1 to 350 kHz.

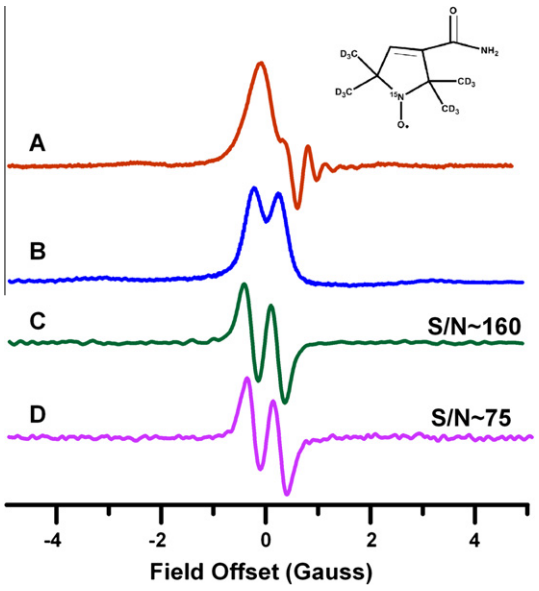

Fig. 6. Comparison of rapid scan and conventional CW EPR spectra of the low-field nitrogen hyperfine line of ^{15}N-mHCTPO. (A) As-recorded sinusoidal rapid scan signal obtained with a scan rate of 1.8 MG/s and microwave power about 80 mW (B_1 = 0.14 G). 1024 averages were recorded in about 0.9 s. (B) Slow-scan absorption spectrum obtained by deconvolution of signal in A. (C) First derivative spectrum obtained by pseudomodulation of the signal in B. (D) Single scan of a conventional field-modulated first-derivative CW EPR spectrum of the same sample, obtained in 0.9 s using 5 mW power, 10 kHz modulation frequency and 0.13 G modulation amplitude. Modulation amplitude, power, and filter were chosen to maximize signal amplitude with less than 2% broadening.

4. Discussion

Power saturation curves for ^{15}N-mHCTPO (Fig. 3) and ^{15}N-PDT (Fig. 4) demonstrate that unsaturated rapid scan spectra can be acquired at higher powers and with higher signal amplitude for the same acquisition time than conventional CW EPR. For a given sample, the bridge and resonator bandwidth were held constant for all measurements, and experiments were performed in a range where noise was independent of power. The signal bandwidth increases linearly with scan rate (Eq. (3)) which requires a higher detection bandwidth for faster scans. If noise is approximately 'white', it increases proportional to the square root of bandwidth. If the scan rate is doubled, and if the data acquisition system is 100% efficient, then twice as many scans can be averaged in the same time. Since noise decreases with the square root of the number of scans, the increase in detector bandwidth is, in principle, compensated by the larger number of scans. The maximum scan rate that does not distort the lineshape is inversely proportional to resonator Q (Eq. (2)). Signal amplitude is proportional to the square root of Q. Lossy samples inherently lower the resonator Q, which provides larger bandwidths that are needed for rapid scans. If a sample is non-lossy, then lowering the Q to permit rapid scans could offset the advantage of scanning faster (Fig. 5A).

The 0.2 mM ^{15}N-PDT sample has a $\Delta B_{pp} \sim 175$ mG and a $T_2^* = 430$ ns $\pm$ 30 ns. It was studied at scan rates up to 4.6 MG/s, which gives BW_{signal} (Eq. (2)) ~28 MHz. The bridge bandwidth was set at 200 MHz. The required BW_{res} is ~56 MHz, and at $\upsilon \sim 9.67$ GHz this corresponds to a $Q \sim 175$. The resonator Q for this experiment was 200. The deconvolved rapid scan spectra at the fastest rate exhibited slight broadening (~3%) even in the linear power region, which is attributed to resonator Q. The rapid scan spectra could still be accurately simulated by accounting for the effect of resonator Q.

The 0.1 mM ^{15}N-mHCTPO sample has a $\Delta B_{pp} \sim 256$ mG for the inhomogeneously broadened proton-hyperfine split lines, and was studied at scan rates up to 1.8 MG/s. T_2^* is about 0.26 μs. The BW_{signal} (Eq. (3)) at the highest rate is ~6.5 MHz, which requires BW_{res} of ~13 MHz. At $\upsilon \sim 9.67$ GHz this corresponds to a $Q \sim 430$. The actual Q for this experiment was 150. Thus, for the ^{15}N-mHCTPO experiment, there was an excess of resonator bandwidth. The bridge bandwidth was set at 20 MHz. No broadening was observed in the deconvolved ^{15}N-mHCTPO rapid scan spectra within the linear power region.

When comparing the signal-to-noise of the fastest rapid-scan data for ^{15}N-mHCTPO with CW EPR, the S/N increased by a factor of 2 with rapid scan (Fig. 6). It is important to note that the current hardware is not yet optimized. Presently, the rapid scans are acquired in a burst sinusoidal mode and data are acquired for only 1 cycle from each burst. Currently, only 4% of the time is being utilized for data acquisition. Thus, we predict that as the hardware for this experiment is improved, the gain in S/N for rapid scan over CW EPR will be much greater.

Acknowledgments

This work was supported in part by NSF IDBR 0753018 and by an NSF Graduate Fellowship to DGM.

References

[1] B.A. Jacobsohn, R.K. Wangsness, Shapes of nuclear induction signals, Phys. Rev. 73 (1948) 942.
[2] J. Dadok, R.F. Sprecher, Correlation NMR spectroscopy, J. Magn. Reson. 13 (1974) 243–248.
[3] M. Tseitlin, G.A. Rinard, R.W. Quine, S.S. Eaton, G.R. Eaton, Deconvolution of sinusoidal rapid EPR scans, J. Magn. Reson. 208 (2011) 279–283.
[4] J.P. Joshi, J.R. Ballard, G.A. Rinard, R.W. Quine, S.S. Eaton, G.R. Eaton, Rapid-scan EPR with triangular scans and Fourier deconvolution to recover the slow-scan spectrum, J. Magn. Reson. 175 (2005) 44–51.
[5] M. Tseitlin, T. Czechowski, S.S. Eaton, G.R. Eaton, Regularized optimization (RO) reconstruction for oximetric EPR imaging, J. Magn. Reson. 194 (2008) 212–221.
[6] M. Tseitlin, A. Dhami, S.S. Eaton, G.R. Eaton, Comparison of maximum entropy and filtered back-projection methods to reconstruct rapid-scan EPR images, J. Magn. Reson. 184 (2007) 157–168.
[7] J.W. Stoner, D. Szymanski, S.S. Eaton, R.W. Quine, G.A. Rinard, G.R. Eaton, Direct-detected rapid-scan EPR at 250 MHz, J. Magn. Reson. 170 (2004) 127–135.
[8] D.G. Mitchell, R.W. Quine, M. Tseitlin, V. Meyer, S.S. Eaton, G.R. Eaton, Comparison of continuous wave, spin echo, and rapid scan EPR of irradiated fused quartz, Radiat. Meas. 46 (2011) 993–996.
[9] D.G. Mitchell, R.W. Quine, M. Tseitlin, R.T. Weber, V. Meyer, A. Avery, S.S. Eaton, G.R. Eaton, Electron spin relaxation and heterogeneity of the 1:1 α, γ-bisdiphenylene-β-phenylallyl (BDPA) : benzene complex, J. Phys. Chem. B 115 (2011) 7986–7990.
[10] S.S. Eaton, G.R. Eaton, L.J. Berliner (Eds.), Biomedical EPR – Part A: Free Radicals, Metals, Medicine, and Physiology, Kluwer Academic/Plenum Press, New York, 2005.
[11] F. Hyodo, S. Matsumoto, N. Devasahayam, C. Dharmaraj, S. Subramanian, J.B. Mitchell, M.C. Krishna, Pulsed EPR imaging of nitroxides in mice, J. Magn. Reson. 197 (2009) 181–185.
[12] M. Tseitlin, A. Dhami, R.W. Quine, G.A. Rinard, S.S. Eaton, G.R. Eaton, Electron spin T_2 of a nitroxyl radical at 250 MHz measured by rapid scan EPR, Appl. Magn. Reson. 30 (2006) 651–656.
[13] R.W. Quine, G.A. Rinard, S.S. Eaton, G.R. Eaton, Quantitative rapid scan EPR spectroscopy at 258 MHz, J. Magn. Reson. 205 (2010) 23–27.
[14] J.S. Hyde, R.A. Strangeway, T.G. Camenisch, J.J. Ratke, W. Froncisz, W-band frequency-swept EPR, J. Magn. Reson. 205 (2010) 93–101.
[15] J.R. Biller, V. Meyer, H. Elajaili, G.M. Rosen, J.P.Y. Kao, S.S. Eaton, G.R. Eaton, Relaxation times and line widths of isotopically-substituted nitroxides in aqueous solution at X-band, J. Magn. Reson. 212 (2011) 370–377.
[16] Y.J. Lin, B.A. Teicher, H.J. Halpern, Synthesis of 4-protio-3-carbamoyl-2,2,5,5-tetraperdeuteromethyl-3-pyrrolin-1-yloxy (mHCTPO): a selectively isotopically labeled compound for use in T_2 spin label oxymetry, J. Labelled Compd. Radiopharm. 28 (1990) 621–631.
[17] H.J. Halpern, M. Peric, T.D. Nguyen, D.P. Spencer, B.A. Teicher, Y.J. Lin, M.K. Bowman, Selective isotopic labeling of a nitroxide spin label to enhance sensitivity for T_2 oxymetry, J. Magn. Reson. 90 (1990) 40–51.
[18] R.W. Quine, D. Mitchell, G.R. Eaton, A general purpose Q-measuring circuit using pulse ring-down. Conc. Magn. Reson. B (Magn. Reson. Engin.) 39B (2011) 43–46.

[19] J.S. Hyde, A. Jesmanowicz, J.J. Ratke, W.E. Antholine, Pseudomodulation: a computer-based strategy for resolution enhancement, J. Magn. Reson. 96 (1992) 1–13.
[20] L. Tan, in: Digital Signal Processing: Fundamentals and Applications, Elsevier, Burlington, 2007, pp. 741–744.
[21] R.W. Quine, G.R. Eaton, S.S. Eaton, Pulsed EPR spectrometer, Rev. Sci. Instrum. 58 (1987) 1709–1723.
[22] J.S. Hyde, W. Froncisz, A. Kusumi, Dispersion electron spin resonance with the loop gap resonator, Rev. Sci. Instrum. 53 (1982) 1934–1937.
[23] M.H. Rakowsky, A. Zecevic, G.R. Eaton, S.S. Eaton, Determination of high-spin iron(III)-nitroxyl distances in spin-labeled porphyrins by time-domain EPR, J. Magn. Reson. 131 (1998) 97–110.
[24] M. Weger, Passage effects in paramagnetic resonance experiments, Bell. Syst. Tech. J. 39 (1960) 1013–1112.